The Effect of Road Unevenness on Cornering Performance of Road Vehicles

Carlo Pastó, Roberto Lot, and Matteo Massaro

***Abstract*—Driving on uneven roads causes wheel load fluctuation that affects tire forces. While cornering, a time-varying vertical load gives a reduction in the (average) lateral force, which may result in the loss of control of the vehicle. The impact of road roughness on maximum achievable lateral acceleration for steady-cornering manoeuvres at constant speed is investigated. Different tyre response models are considered.**

***Index Terms*—uneven-roads, cornering, lateral-dynamics, handling, understeer-gradient.**

I. Introduction

Wheel load fluctuations have a major role on tire force generation and are significantly affected by road roughness. While the vehicle is cornering, time-varying load causes a loss in the average lateral force and as a result the limit lateral acceleration reduces as well. The main causes of the phenomenon are summarized and simulation results of a full-car model riding on different road profiles are carried out. A novel formula is introduced to evaluate the lateral performance of the vehicle. The work is organised as follows. In section II we give insights about the phenomena by reporting the most important contributions of the literature; in III the steer property diagram along with road and tyre modelling are presented, together with the effect of road roughness on a quarter car model; simulation results of the full vehicle are discussed in section IV.

II. Literature review

The lateral force variation due to load fluctuations was measured in the past by some authors [1]–[4], who set tires at fixed slip angle on a test bench. The experiments showed a loss in the average force which can be split in its ”static” and ”dynamic” parts. The ”static” loss is based on the fact that the cornering stiffness is sub-linear with load variation amplitude. The ”dynamic” loss is caused by the lag in the side force response to load fluctuation. This mechanism is space dependent rather than time dependent, and can be modelled using a first-order differential equation, whose delay is associated to the relaxation length [2]. This parameter depends on the contact length, and thus is also related to the wheel load.

Manuscript received March 23, 2021; revised May 4, 2021. This work was partially supported by grant ”Programma Operativo Regionale F.S.E. 2014-2020 Regione Veneto In sinergia con il Fondo Europeo di Sviluppo Regionale POR 2014-2020, Cod. progetto 2105-0053-1463-2019 CUP C94E19000850008”

Carlo Pastò is Research Fellow of the Department of Industrial Engineering (DII), Università degli Studi di Padova, Padua, 35131 Italy, e-mail: carlo.pasto@unipd.it.

Roberto Lot is Associate Professor of the Department of Industrial Engineering (DII), Università degli Studi di Padova, Padua, 35131 Italy, e-mail: roberto.lot@unipd.it

Matteo Massaro is Associate Professor of the Department of Industrial Engineering (DII), Università degli Studi di Padova, Padua, 35131 Italy, e-mail: matteo.massaro@unipd.it

In [4] Takahashi and Pacejka developed a linear string-based model for transient responses. The wheel load effect previously discussed along with tyre inertial properties were implemented in the model. Good experimental agreement is reported with sinusoidal load input. Some years later, the same authors enhanced the tyre model to make it suitable for large sideslip conditions, in order to properly represent the faster response of the tyre close to adhesion limit [5]. A number of numerical issues of the model were analysed by Takahashi and Hoshino [6] to avoid computational instability. A more sophisticated solution to the problem was introduced by Pacejka and Besselink in [7], through the introduction of the contact patch mass.

The lateral force loss is low when the fluctuation is small, but it increases in non-linear fashion with wheel load amplitude and spatial frequency [3], [4]. As a consequence also the maximum achievable average lateral force reduces with the load fluctuation. When the tyre is attached to a car, the actual input is the road elevation with the wheel load depending on tyre stiffness and suspension characteristics. In addition, the sideslip is no more constant. New interactions are introduced, therefore a variation of lateral dynamics is expected. Several authors have dealt with this aspect. Further experimental investigations were carried out in [3] by performing a steady-cornering manoeuvre with a vehicle whose wheels were eccentrically mounted. The author focused on stability for different combinations of axle eccentricity and evaluated the yaw velocity gain for increasing forward velocity, concluding that vehicle understeering increases when greater load fluctuations are on the front axle, and the other way around. This suggests that suspension design has major role in the stability of the vehicle, as the wheel load fluctuation depends on stiffness and damping of the suspension itself.

A full-car model was simulated by Rill [8], who implemented a proportional driver control to accomplish a constant path curvature trajectory at increasing forward velocity. The first simulation results were summarised with the steer property diagram (steer angle vs. lateral acceleration): the data are quite sparse for poor roads, while get closer for good roads. However no quantitative considerations are found about the mean trend and lateral acceleration limit with respect to the road considered.

In [9] the lane-change manoeuvre is considered for handling performance on uneven road. Lozia simulated a full-car model and showed that the lateral acceleration gain and yaw rate gain always reduce with increasing uneveness. The vehicle trajectory is the focus of the work, which is shown to dramatically depend on road and vehicle’s stability characteristics in the case the steer is controlled in open-loop. The same author in [10] reported simulations similar those carried out by Rill [8], finding good agreement.

In [11], Mühlmeier simulated a vehicle in steady-

ISBN: 978-988-14049-2-3
ISSN: 2078-0958 (Print); ISSN: 2078-0966 (Online)

cornering, for increasing path radius, with a proportional driver control. He employed a rigid-belt based tyre model. The steering wheel angle and the vehicle slip angle are plotted against the lateral acceleration for five load fluctuations. The results show that the slip angle increases, while the lateral acceleration limit reduces with increasing load fluctuations.

Ookubo et al. [12] proposed the standard deviation of the instantaneous stability factor as a index to evaluate vehicle 'traceability' for a vehicle driving on a constant path curvature. This index is suggested by the authors for a subjective rating of the experimental tests conducted by different drivers.

Mashabi and Crolla reported in [13] findings about step-steering response simulations of a full-car model provided with a 1st order tyre model, whose delay is accounted on lateral force. Results show that the lateral force loss due to load variations is compensated by the increase of the side slip. Given that the tyre sideslip saturates earlier on rougher roads, the maximum lateral force is obtained at lower lateral accelerations. The authors show that the understeer gradient is almost constant for small accelerations and practically independent from the road profile when riding on moderate roughness.

More recently, Takahashi [14] simulated a full-car with tyre model based on [5]. By experimental tests and fitting of the tyre response, the author obtained very good agreement with the numerical simulations for wavelengths above about 1 m. Takahashi simulated also two maneuvers at constant speed on sinusoidal undulations: sinusoidal steer and step steer input were considered. It has been shown that at short wavelength excitation the average lateral acceleration of the car is higher with respect to a smooth road due to the transient property of the tyre, while on long wavelength it decreases.

In sum, several approaches have been employed to evaluate both the lateral acceleration limit and the stability of a vehicle as function of the load fluctuation, with different vehicle and tyre models, with results that are not always in agreement one-another. In this paper we evaluate the lateral performance adopting the lateral acceleration against steering angle diagram, i.e. the steer property diagram. To do so, the car is simulated with a constant steer rate – the steer angle as a function of time is a ramp – at constant forward speed. This representation gives explicit information about both maximum achievable lateral acceleration and the understeering tendency of the vehicle. Before that, a pragmatic quarter car model is presented to highlight the basic vehicle behaviour on uneven roads.

TABLE I
SYMBOLS

Symbol	*description*
a_y	Lateral acceleration
c	Suspension damping
$C_{F\alpha}$	Cornering stiffness
C_y	Lateral stiffness
F_y	Lateral force
F_z	Normal force
k	Suspension stiffness
R	Path radius
U	Understeer gradient
w	Wheelbase
v	Lateral deflection
V	Longitudinal velocity
α	Slip angle
α'	Transient slip angle
β	Attitude angle (vehicle slip angle)
δ	Steer angle
δ_{kin}	Kinematic steer angle
ΔF_z	Lateral load transfer
κ	Path curvature
σ_0	Relaxation length ($\alpha = 0$)
σ^*	Relaxation length
Suffixes	
f,r	front, rear
l,r	left, right
ss	steady state
α	lateral
s	sprung/suspension
t	tyre
u	unsprung

III. SIMULATION MODELS

A. Background and purpose

The steady-cornering test is a widespread approach to experimentally evaluate the handling performance of a vehicle; its definition is reported in the ISO Standard [15]. Three methods are suggested to carry out the manoeuvre: constant radius, constant steer angle and constant speed. Even if the methods are declared equivalent for the Standard, some discrepancies in the results may arise for several non-linear effects, e.g. a variation of the forward velocity causes a different wheel excitation, aerodynamic effects, etc. The three methods can be simulated, respectively, by providing an increasing speed velocity for a constant radius, by implementing a PID driver control for the constant steer angle method, and by providing the steering angle as a function of time for the constant speed test. The latter method is open-loop, and the sideslip variations are only caused by the road unevenness. In contrast, the closed-loop control leads to variations due to both road undulation and steering compensations.

The steer property diagram can be described using the following relationship in the linear range [16]:

$$\delta = \delta_{kin} + U \cdot a_y \tag{1}$$

with the general definition of understeer gradient

$$U = \frac{d\delta}{da_y} - \frac{d\delta_{kin}}{da_y} \tag{2}$$

defined in steady-state conditions. Equation (1) can be rewritten as follows:

$$\delta = \frac{w}{R} + U \cdot \frac{V^2}{R} = w \cdot \kappa + U \cdot V^2 \cdot \kappa \tag{3}$$

where the first right-hand-side term is δ_{kin}. Equation (3) exhibits the steer angle δ dependency on path curvature κ and forward velocity V. If the path curvature is varied then the relationship in equation (3) passes through the origin, while in the constant path curvature case a non-zero steer angle is expected at negligible lateral acceleration. In this work the steady cornering is achieved by applying a steering ramp at constant forward velocity.

B. Road

Road irregularities are modelled with the well-know stochastic approach described in [17], which defines the

ISBN: 978-988-14049-2-3
ISSN: 2078-0958 (Print); ISSN: 2078-0966 (Online)

elevation of the road profile in terms of its power spectral density (PSD) as follows

$$\Phi_D = \Phi_{D0}(\Omega_0) \cdot \left(\frac{\Omega}{\Omega_0}\right)^{-w} \tag{4}$$

The classic wheelbase filter is applied [18], so that the rear tyres follow the same path of front axle with constant spatial delay.

C. Tyre Model and Quarter Car Model

It has been previously discussed that there are two main contributions to the average lateral force reduction: the "static" loss which is due to non-linear load tire characteristics such as the cornering stiffness and the friction coefficient, and the "dynamic" loss that is the result of the space-delayed force response of the tyre due to the relaxation length.

The relaxation length concept was introduced by von Schilippe et al. [19] who developed the string model and proposed the first-order differential equation for the deflection of the string at the leading edge, which reads in pure slip conditions:

$$\frac{dv}{ds} + \frac{1}{\sigma} v = \alpha \tag{5}$$

The previuos expression can be rewritten in terms of transient slip angle, assuming that the relaxation length is a function of tyre load only:

$$\sigma \frac{d\alpha'}{ds} + \left(\frac{d\sigma}{dF_z}\frac{dF_z}{ds} + 1\right)\alpha' = \alpha \tag{6}$$

If the first term in the brackets is negligible, it holds:

$$\sigma \frac{d\alpha'}{ds} + \alpha' = \alpha \tag{7}$$

In the linear range, the differential equation can be rewritten again with the transient lateral force by multiplication by the (assumed constant) cornering stiffness:

$$\sigma \frac{dF_y'}{ds} + F_y' = F_y \tag{8}$$

The global loss can be estimated employing a quarter car model (QCM) whose mechanical parameters are in table II while the tyre curve are shown in figure 1. The QCM is simulated as it rides on a ISO Road at several constant slip angles. The average lateral force is computed for each sideslip and plotted in figure 2.

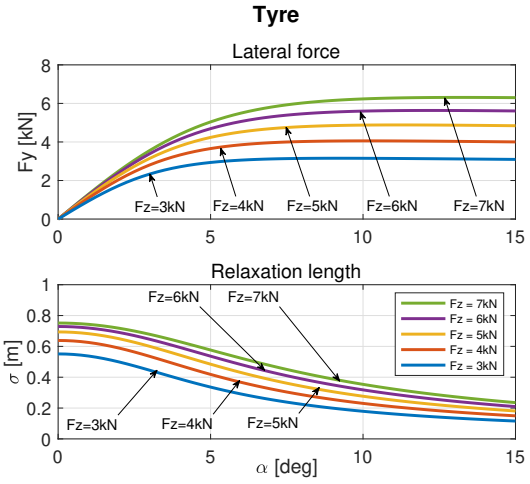

Fig. 1. Lateral force F_y and relaxation length σ of the tyre at normal loads F_z increasing from 3 (blue) to 7 (green) kN, by steps of 1 kN.

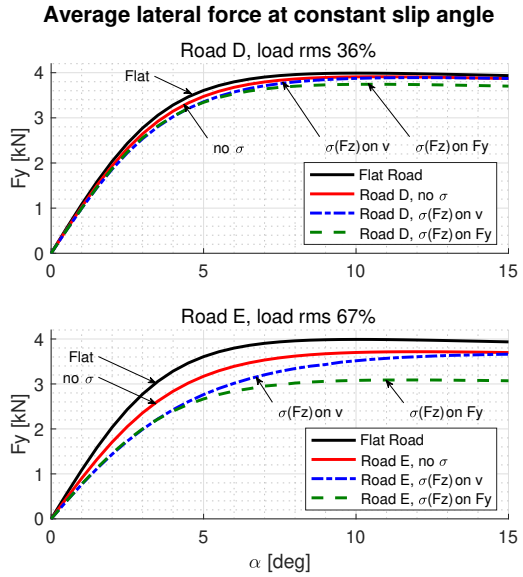

Fig. 2. Average lateral force of a QCM riding on uneven road at constant sideslip angle.

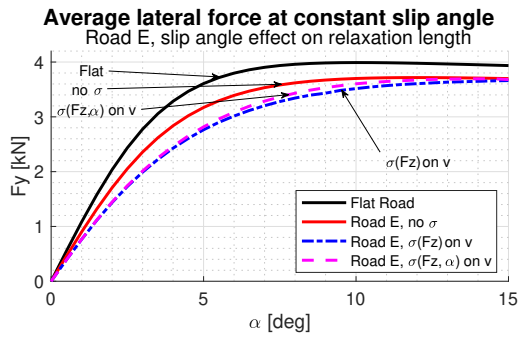

Fig. 3. Effect of slip angle dependency of relaxation length on average lateral force for a QCM riding on uneven road at constant slip angle.

ISBN: 978-988-14049-2-3
ISSN: 2078-0958 (Print); ISSN: 2078-0966 (Online)

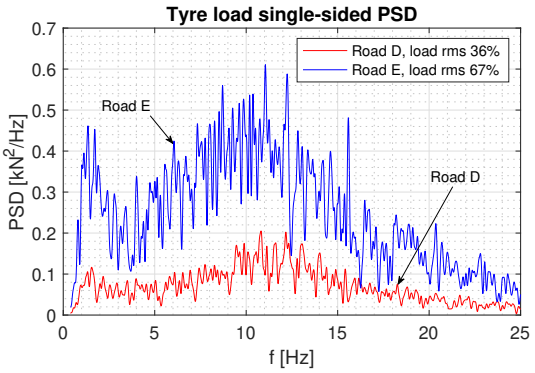

Fig. 4. Tyre load single-sided PSD for the QCM.

In figure 2 the black line represents the flat road condition (no losses), the red line is the average lateral force subjected to the "static" loss only, and the blue and green lines are the average lateral forces when equations (5) and (8) are used. Equation (7) – not shown – clearly gives result equal to the red line, as the slipangle is kept constant. In these conditions no substantial loss can be observed for ISO Road A, B and C all over the slip range. As the wheel-load rms becomes larger, i.e. on ISO Road D and E, 36% and 67% load-fluctuation rms respectively, the loss is no more negligible. Tyre load PSD are reported in figure 4. Figure 2 clearly shows that the average cornering stiffness is affected by load fluctuations and both relaxation length expressions lead to the same result until the slip angle is small. The global loss reaches its maximum when the lateral force approaches its peak value, then at higher slips equation (8) is no longer applicable and the "dynamic" loss reduces and becomes negligible as blue and red lines come together.

A relaxation length dependent on slip was introduced in [5], [6]. This feature can be accomplished with the following set of equations [5], [6], [20]:

$$\frac{dv}{ds} + \frac{1}{\sigma^*_\alpha} v = \tan\alpha \tag{9}$$

$$\alpha' = \arctan\frac{v}{\sigma^*_\alpha} \tag{10}$$

$$\sigma^*_\alpha = \frac{\sigma_{\alpha 0}}{C_{F\alpha}} \frac{F_y}{\tan\alpha'} \tag{11}$$

$$\sigma_{\alpha 0} = \frac{C_{F_\alpha}}{C_y} \tag{12}$$

$$F_y = F_{y,ss}(\alpha', F_z) \tag{13}$$

The lag response is accounted with the first order differential equation for the lateral deflection v, equation (9), where σ^*_α is the slip-dependent relaxation length. This is obtained using (11), starting from the relaxation length at small slips $\sigma_{\alpha 0}$, which is defined in (12). The istantaneous lateral force is computed with the Magic Formula (13) using the transient slip angle α' in (10).

An alternative formula to account for the variation of the relaxation length with the sideslip is reported in [5], [6]:

$$\sigma^*_\alpha = \sigma_{\alpha 0} \frac{\sin(\arctan C_\sigma \alpha')}{C_\sigma \alpha'} \tag{14}$$

where C_σ is a coefficient that can be obtained from the fitting of equation (11).

Regardless the formulation employed, i.e. either (11) or (14), this set of equations needs iterations to be solved considering that the relaxation length is a function of the transient angle, that is the ratio of the lateral deflection to the relaxation length itself. The numerical solution may fail when rapid load reduction occurs at high slips and low tyre loads, which is very likely when ISO Road D and E are used. For this reason, in this work the relaxation length is computed through the steady state slip angle α in place of the transient slip angle α', as follows:

$$\sigma^*_\alpha = \frac{\sigma_{\alpha 0}}{C_{F\alpha}} \frac{F_{y,ss}(\alpha, F_z)}{\tan\alpha} \tag{15}$$

Furthermore the new implemented equation allows to avoid iterations to solve the set of equations: it is thus convenient from a computational point of view.

In figure 3 the effect of the sideslip angle on relaxation length (magenta line) is compared with the first definition (blue line), and, as expected, at higher slips the dynamic loss reduces. The transient lateral force may be observed by simulating a QCM riding at costant slip angle above two consecutive increasing and decreasing steps, spaced enough to reach steady state between them. Figure 5 shows the difference ΔF_y between the actual and steady lateral force: again that the mean lateral force is reduced.

Fig. 5. Dynamic response of the tyre for a step road, Δz=10mm, α=5deg, $F_{y,0}$=3.57kN

D. Vehicle Model

The vehicle is modelled as main sprung body and four unsprung masses. Suspension stiffness and damping are computed using the following equations:

$$k_s = \frac{m_s m_u}{(m_s + m_u)^2} \cdot k_t \tag{16}$$

$$c_s = \sqrt{\frac{m_s^3 m_u k_t}{(m_s + m_u)^3}} \tag{17}$$

that represent the optimum performance parameters [21]. The weight distribution is unequal, so that the vehicle is understeering since tyres are all the same and the front axle is more loaded. The steering assembly is assumed to be rigid, with identical steer angle on wheels.

ISBN: 978-988-14049-2-3
ISSN: 2078-0958 (Print); ISSN: 2078-0966 (Online)

TABLE II
VEHICLE CHARACTERISTICS

Parameter	Description	Value	Units
c_{sf}	front suspension damping	2.32	kNs/m
c_{sr}	rear suspension damping	2.29	kNs/m
k_{sf}	front suspension stiffness	15.5	kN/m
k_{sr}	rear suspension stiffness	16.5	kN/m
l_f	front axle position wrt cog	1.2	m
l_r	rear axle position wrt cog	1.3	m
h	cog heigth	0.45	m
m_t	total mass	1600	kg
m_u	unsprung mass	35	kg
t_f	half front track width	0.8	m
t_r	half rear track width	0.8	m
I_{xx}	pitch inertia	500	kg m^2
I_{yy}	roll inertia	2300	kg m^2
I_{zz}	yaw inertia	2500	kg m^2
w	wheelbase	2.5	m

The vehicle has 10 degrees of freedom, namely yaw, pitch, roll, heave, longitudinal position, lateral position, and four unsprung vertical travels, plus the steering that is a controlled input. The characteristics of the vehicle are summarised in table II.

IV. CORNERING PERFORMANCE OF A CAR

The steady cornering maneuver has been carried out to evaluate the lateral performance of the vehicle, whose characteristics are reported in table II. A steer angle ramp function has been applied, having 5 deg final value at 50 s simulation, 100 kph constant forward speed. The results of the vehicle on an even road have been compared when running on ISO D and ISO E roads. In figure 8 is reported the vehicle sideslip angle, which clearly increases with road roughness. Figure 6 and 7 depict normalized probability distribution of normal load (contact point) and lateral force of the tyres for the front axle (the rear axle presents approximately the same shape) at the limit lateral acceleration; the vertical lines represent the values on the flat road. These figures show that a non-gaussian lateral force distribution is obtained despite the wheel load is normally distributed (until the tyre is not jumping) due to non-linear response of the tyre.

The steer property diagrams are shown in figure 9: in the upper graph the simulation results are plotted, while in the lower one, the trend has been fitted using the novel formula

$$\delta = U_0 \cdot a_y \cdot \frac{1}{1+\chi} \cdot \left(1 + \frac{\chi}{1-(a_y/a_{y,lim})^2}\right) \qquad (18)$$

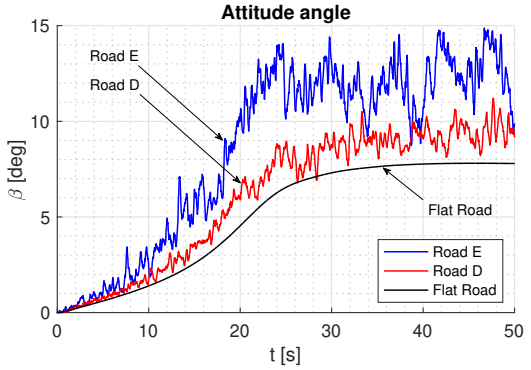

Fig. 8. (Full-car model) Effect of road unevenness on attitude angle.

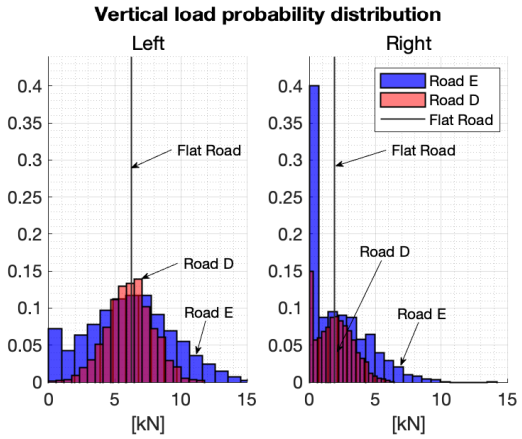

Fig. 6. (Full-car model) Wheel load normalized distribution for ISO Road D (Red) and E (Blue) - purple histogram intersection

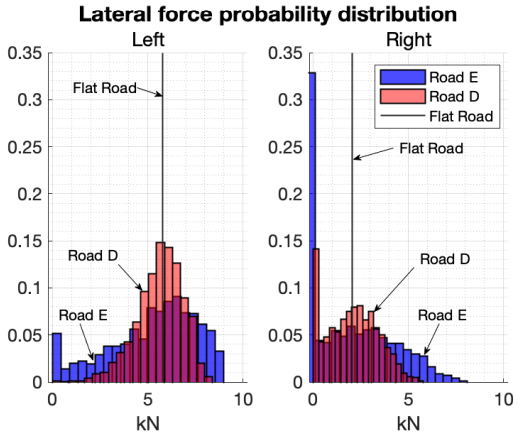

Fig. 7. (Full-car model) Lateral force probability distribution for ISO Road D (Red) and E (Blue) - purple histogram intersection

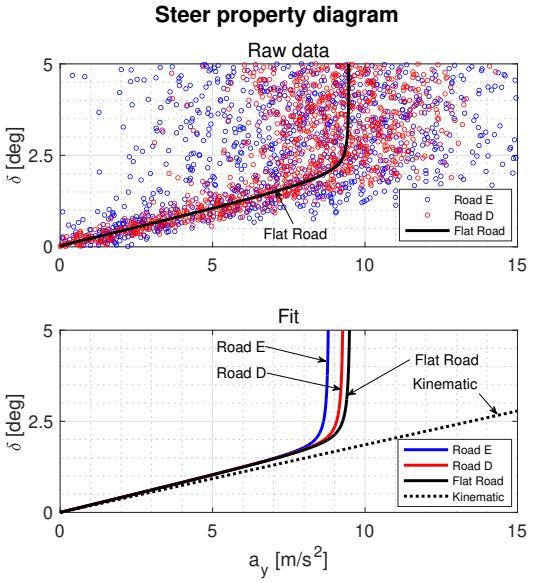

Fig. 9. (Full-car model) Steer property diagram: upper graph depicts raw data - road E (blue marker) gives sparser results than road D (red marker), lower graph curves are obtained using fitting equation 18. $U_0 = 0.205 \quad [deg \cdot s^2/m]$, $\chi = 0.02$, $a_{y,lim} = 8.84, \quad 9.32, \quad 9.55 \quad [m/s^2]$.

ISBN: 978-988-14049-2-3
ISSN: 2078-0958 (Print); ISSN: 2078-0966 (Online)

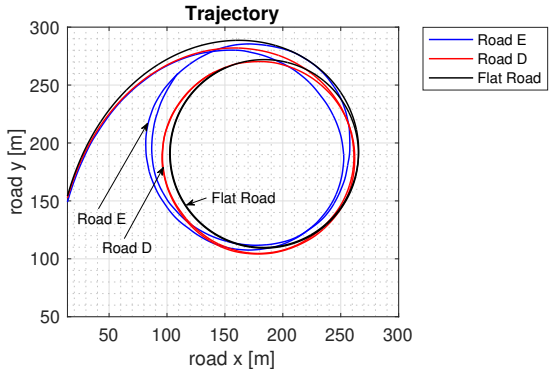

Fig. 10. (Full-car model) Effect of road unevenness on minimum path radius

The fitted curve represents the average case, so the lateral performance may instantaneously be worse or better. The coefficient U_0, which equals the understeer gradient at small slip angles, has no changes for all the roads, and so also the "curvature coefficient" χ. The road unevenness causes only a reduction in the limit acceleration: as a consequence the path radius increases, figure 10.

V. Conclusion

This work discussed how road roughness severity causes a worsening in the lateral performance of a four-wheeled vehicle. Firstly, a detailed literature review has been given. The effect of uneven roads on average lateral force has been shown for the simple quarter-car model, then the full vehicle performance has been evaluated by simulating the steady cornering manoeuvre at constant speed and increasing steer angle. The steer property diagram has been employed to summarise the performance of the car, which shows that the road unevenness affects predominately the limit lateral acceleration, while at small slips the understeer gradient is not significantly affected by road excitations. A novel formula has been introduced to fit the steer property diagram curve, which is useful to estimate the lateral acceleration limit and the understeer gradient.

Acknowledgment

Authors would like to thank Matteo Bova for his contribution about tyre modelling.

References

[1] H. Kurtz, "Seitenfuhrungs kraft des kraftwagen rades bei wechelnder radlast (lateral control force on vehicle wheels for the case of alternating wheel loads)," *Automobiltechnische Zeitschrift - ATZ*, vol. 60, no. 5, 1958.

[2] W. Metcalf, *Effect of a Time-varying Load on Side Force Generated by a Tire Operating at Constant Slip Angle*, ser. SAE-630150, 1963.

[3] M. Mitshke, "The performance of passenger cars on uneven roads (fahrverhalten von personenkraftwagen auf unebener strasse)," *Automobiltechnische Zeitschrift - ATZ*, vol. 85, no. 11, pp. 695–698, 1983.

[4] T. Takahashi and H. B. Pacejka, "Cornering on uneven roads," *Vehicle System Dynamics*, vol. 17, no. sup1, pp. 469–480, 1988. [Online]. Available: https://doi.org/10.1080/00423118808969288

[5] H. B. Pacejka and T. Takahashi, "Pure slip characteristics of tyres on flat and on undulated surfaces," *Advanced Vehicle Control*, pp. 360–365, 1992.

[6] T. Takahashi and M. Hoshino, "The tyre cornering model on uneven roads for vehicle dynamics studies," *AVEC '96 International Symposium on Advanced Vehicle Control*, pp. 941–954, 1996.

[7] H. B. Pacejka and I. J. M. Besselink, "Magic formula tyre model with transient properties," *Vehicle System Dynamics*, vol. 27, no. 1, pp. 234–249, 1997. [Online]. Available: https://doi.org/10.1080/00423119708969658

[8] G. Rill, "Steady state cornering on uneven roadways," in *SAE International Congress and Exposition*. SAE International, mar 1986. [Online]. Available: https://doi.org/10.4271/860575

[9] Z. Lozia, "An analysis of vehicle behaviour during lane-change manoeuvre on an uneven road surface," *Vehicle System Dynamics*, vol. 20, no. sup1, pp. 417–431, 1992. [Online]. Available: https://doi.org/10.1080/00423119208969413

[10] ——, "A comparison of driver steering activity during motion on an even and uneven road surface," *Vehicle System Dynamics*, vol. 23, no. sup1, pp. 322–333, 1994. [Online]. Available: https://doi.org/10.1080/00423119308969524

[11] M. Muehlmeier, "Evaluation of wheel load fluctuations," *International Journal of Vehicle Design*, vol. 16, pp. 397–411, 1995. [Online]. Available: https://doi.org/10.1504/IJVD.1995.061945

[12] N. Ookubo, H. Moroizumi, and K. Isoda, "Handling characteristics on uneven road surface in a turn," *Jsae Review*, vol. 21, pp. 252–254, 2000.

[13] B. Mashadi and D. Crolla, "Influence of ride motions on the handling behaviour of a passenger vehicle," *Proceedings of The Institution of Mechanical Engineers Part D-journal of Automobile Engineering*, vol. 219, pp. 1047–1058, 09 2005.

[14] T. Takahashi, "The influence of tyre transient side force properties on vehicle lateral acceleration for a time-varying vertical force," *Vehicle System Dynamics*, vol. 56, pp. 1–19, 09 2017.

[15] "Passenger cars — steady-state circular driving behaviour — open-loop test methods," International Organization for Standardization (ISO), Geneva, CH, Tech. Rep., 2012.

[16] "Vehicle dynamics terminology," Tech. Rep., jan 2008.

[17] "Mechanical vibration – road surface profiles - reporting of measured data," International Organization for Standardization (ISO), Geneva, CH, Tech. Rep., 2016.

[18] D. J. N. Limebeer and M. Massaro, *Dynamics and optimal control of road vehicles*. Oxford: Oxford University Press, 2018.

[19] B. Schlippe and R. Dietrich, "Das flattern des pneumatischen rades (eng. ver. : Shimmying of a pneumatic wheel)," *Lilienthal Gesellschaft für Luftfahrtforschung (NACA TM 1365)*, 1941 (1953).

[20] H. B. Pacejka, *"Tire and Vehicle Dynamics"*, 3rd ed. Butterworth-Heinemann, 2012, pp. 258–260,336–338. [Online]. Available: https://doi.org/10.1016/C2010-0-68548-8

[21] R. Lot and J. Sadauckas, *"Motorcycle Design"*, 2021.

ISBN: 978-988-14049-2-3
ISSN: 2078-0958 (Print); ISSN: 2078-0966 (Online)